Research Article

Evaluation and minimization of moment coefficient of tall buildings with trilateral cross-section via a surrogate model

M. Noormohamadian[1] · E. Salajegheh[1]

Received: 30 July 2020 / Accepted: 30 December 2020 / Published online: 28 January 2021

Abstract
Wind load is commonly regarded as the dominant lateral load in designing tall buildings. Thus, it is of necessity to investigate the parameters affecting wind-induced loads. One of these parameters is the exterior shape of tall building, which using its aerodynamic shape modifications, wind loads, can be decreased. In this research, the exterior shape of different tall buildings with trilateral cross-section is constructed via the polynomial parameterization method. The advantage of the proposed method in producing the building geometry is that it is able to apply all aerodynamic modifications to triangular buildings. Then, the effect of each geometrical parameter on the moment coefficient along the drag is investigated as the aerodynamic response of tall buildings. Using geometric parameters screening, it was found that two geometrical parameters (T, b_1) have the maximum impact on the aerodynamic response of the tall buildings which apply twist and curved sides modifications, respectively. Then, using the polynomial regression method, explicit relation of the mean moment coefficient in terms of these two geometrical parameters is illustrated using a third-order polynomial, which can be used as a surrogate model to evaluate the moment coefficient instead of computational fluid dynamic analysis. The surrogate model can significantly reduce the computational cost, and operate as an appropriate guide for building designers to investigate the effect of building geometrical variables on aerodynamic performance. Finally, the minimum point of the proposed model is determined as the optimal shape of the tall building. In addition, a comparative analysis of the aerodynamic responses of the optimal model with the basic triangle model shows that the moment coefficient is reduced by 56%. This demonstrates the considerable effect of these two geometrical parameters in improving the aerodynamic performance.

Keywords Tall building · Aerodynamic modifications · Computational fluid dynamic · Polynomial regression method · Shape parameterization

1 Introduction

The wind-induced load is customarily considered as the dominant lateral load in the design of some cases of civil structures, including suspension bridges and tall buildings. Such loads can be lessened by structure shape modifications.

Much research has been performed in this regard. For example, the references [1, 2] examine how bridge deck cross-section modification affect the aerodynamic performance of the bridge, and the results corroborate that modification of suspension bridge deck cross-section can significantly improve aerodynamic performance and aerodynamic stability. Furthermore, aerodynamic modifications of the exterior shape of tall buildings can reduce wind loads to much extent. These modifications are performed in two ways, including cross-section modifications (minor ones) and modifications along the building height

✉ M. Noormohamadian, mehdi.noormohamadian@gmail.com | [1]Department of Civil Engineering, Shahid Bahonar University of Kerman, Kerman, Iran.

SN Applied Sciences (2021) 3:234 | https://doi.org/10.1007/s42452-020-04128-5

(major ones). Corner modifications fall into the category of minor modifications, and different types of this modification, such as chamfered [3–6], rounded [3, 4, 7, 8] and recessed [6, 7] have been examined in various research. There is also an increasing number of research on major aerodynamic modifications such as tapering [9–15], setback [9, 14, 15], twisting [11, 16, 17] and opening modifications [18–20].

Tamura's group [21, 22] investigated the effect of minor and major aerodynamic modifications on some cross-sections, including triangles, squares, rectangles, etc. The results obtained are not only useful for the initial designing of tall buildings but also can be utilized as a valuable future research database on tall buildings. While the majority of the studies reinstate the benefits of aerodynamic modifications, they have adverse effects in some cases, and it would be required to be very careful in selecting the size and type of modifications [10, 18].

One research that examines aerodynamic modifications on triangular tall buildings is the one authored by Bandi et al. [23]. They applied five different models of aerodynamic modifications on a triangular building, and compared their responses with each other, and investigated the effect of each of these modifications separately on the reduction of aerodynamic response. Furthermore, Daemei et al. [24]. applied six different models of aerodynamic modification separately on a triangular building, and examined their effect on aerodynamic response. However, the effect of simultaneous application of different aerodynamic modifications has not been considered in the research.

To select an appropriate and effective aerodynamic modification, different combinations of size and type of modifications are required to be created and aerodynamic responses of different models to be compared. This entails analysis of various combinations via some techniques such as computational fluid dynamic (CFD). This technique necessitates a high computational cost. Thus, researchers have always endeavored to reduce these costs. One approach is to use the 2D model instead of the 3D model, which reduces the computational domain. Kareem et al. [25] offered a method to optimize the corner shape of tall buildings to reduce drag and lift coefficients via 2D CFD models. This method is highly effective in overcoming the computational cost related to the iteration method needed for optimization. Another method is the application of the surrogate models to evaluate the aerodynamic response. Surrogate modeling has been developed to produce approximate functions for expensive numerical and experimental simulations such as aerodynamic coefficient evaluation in wind tunnel tests and CFD simulation in wind engineering problems. There are various surrogate modeling methods such as artificial neural networks (ANN), polynomial regression, Kriging functions, and radial basis functions (RBFs).

Elshaer et al. [26, 27] used the ANN model as a surrogate model to evaluate moment coefficients as objective functions in the optimization process, and they showed that a surrogate model could reduce computational time, the ANN model is able to fit into the training database having a correlation coefficient of close to one, and can greatly speed up the optimization process. Bernardini et al. [28] analyzed the Kriging model efficiency as a surrogate model to evaluate objective functions (drag and lift coefficients) in the optimization process, and they demonstrated the ability of this model in terms of computational time saving and acceptable accuracy in the approximation of objective functions. The authors parameterized the shape of the square cross-sections using the spline method and they used the position of two control points (as design variables) to optimize the corner shape of a square cross-section during the optimization process. Krajnovic [29] investigated the aerodynamic optimization of train geometry in a multi-objective optimization problem, and used second-order polynomials (response surface methodology, RSM) to calculate the aerodynamic response of the train in the optimization process. Hanan et al. [30] investigated optimization of an S-shaped transition duct, and the pressure coefficient was taken into account as the objective function in the optimization process. Then, the coefficient was estimated using the response surface method at each iteration step of the optimization process, and it was found that the approximate function considered is of good accuracy. Immonen [31] studied the shape optimization of the airfoil, and the drag and lift coefficients were taken as the objective functions. Additionally, using the RSM, the relationship between airfoil shape parameters and coefficients was explained, which lift coefficient was accurately approximated via linear model, and drag coefficient approximated via quadratic model. Nariman [32] used a quadratic polynomial (RSM) to approximate the kinetic energy and lift force generated on the bridges deck. He also used the latin hypercube experimental method as a sampling point method to construct the model. The results showed that the approximation function used has the coefficient $R^2 = 99.99\%$, which indicates a very high accuracy in kinetic energy and lift force approximation.

A surrogate model is presented in the current article to approximate the mean moment coefficient along the drag for tall buildings with trilateral cross-sections based on the polynomial regression method. The proposed approximation function is based on the geometric parameters of the exterior shape of the building. To construct the exterior shape of the buildings, the polynomial method is used for shape parameterization. The suggested method can investigate various aerodynamic modifications on the exterior

of a tall building with trilateral cross-sections using seven geometrical parameters. Accordingly, it is possible to study the effect of simultaneous application of several aerodynamic modifications on triangular buildings, which were not considered in previous studies on triangular buildings. The issue is described in the following section in more detail. Furthermore, the proposed approximation function of the moment coefficient using the polynomial regression method has good accuracy and it can be used instead of CFD analysis to examine the aerodynamic performance of the tall buildings with trilateral cross-sections. In the construction of this proposed surrogate model, the effect of building height changes is not considered, and this model can be used for tall buildings with specified heights and boundary conditions.

2 Geometry description

Geometry generation is the first important step to investigate the effects of shape on aerodynamic responses, and the exterior shape of the building can be explained by using several geometrical parameters. Choosing a suitable geometric description technique enables the designer to explore the optimal shape in a large search space. There are various techniques for shape parameterization, such as domain element, polynomial and spline, free form deformation (FFD), and basis vector [33]. In the present study, the polynomial method was used for modeling the exterior shapes of tall buildings, with seven geometric parameters considered as input factors. Therefore, a quadratic polynomial was utilized to define the cross-section, and a cubic polynomial to define the elevation. The issue is explained in the next two sections.

2.1 Vertical profile

The vertical profile (elevation) of the building is defined by a third-order polynomial (Eq. 1). The polynomial coefficients a_0, a_1, a_2, and a_3 represent four input factors. In Eq. 2, bz_i represents y (z) at the height of z_i. Figure 1 represents an example of the vertical profile of the building.

$$y(z) = a_0 + a_1 z + a_2 z^2 + a_3 z^3 \tag{1}$$

$$b_{z_i} = a_0 + a_1 z_i + a_2 z_i^2 + a_3 z_i^3. \tag{2}$$

2.2 Horizontal profile

The horizontal profile or cross-section of the building was defined by a second-order polynomial, and the polynomial coefficients b_0 and b_1 are two input factors. Equation 3 shows the curved sides of the modified cross-section, as represented in Fig. 2.

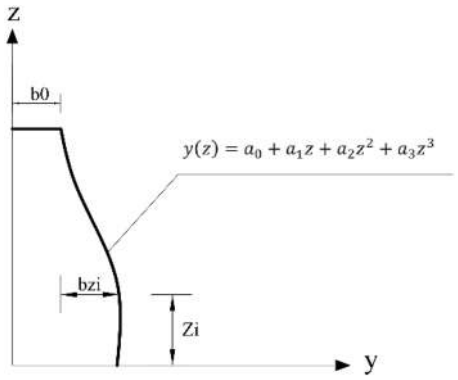

Fig. 1 Vertical profile geometry

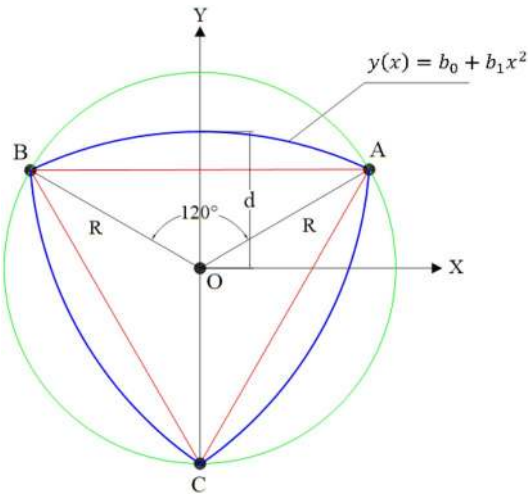

Fig. 2 Horizontal profile geometry

Points A and B are two vertices of the triangle, and their coordinates are obtained by Eqs. 4 and 5. Given that the basic triangle is an equilateral triangle, the closed-form of the cross-section is obtained via mirroring the curve AB with respect to the lines OA and OB, as shown in Fig. 2. To determine the allowable range of the shape changes, a circle with radius R is defined that passes through points A, B and C (triangle vertices).

$$y(x) = b_0 + b_1 x^2 + b_z \tag{3}$$

$$x_A = Rcos(30^\circ), y_A = Rsin(30^\circ) \tag{4}$$

$$x_B = -Rcos(30^\circ), y_B = Rsin(30^\circ). \tag{5}$$

Using the six geometric parameters b_0, b_1, a_0, a_1, a_2, a_3, the exterior shape of the tall building can be constructed,

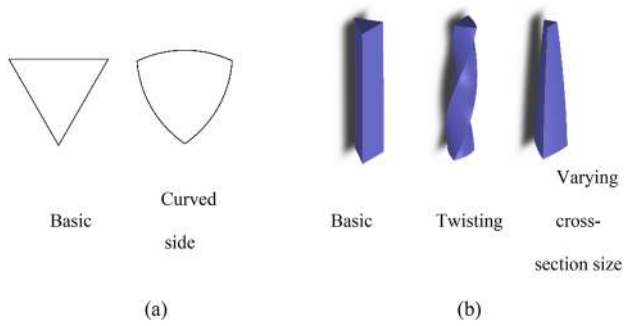

Fig. 3 Types of modifications applied to the exterior forming process. **a** Cross section and **b** along the building height

and the parameters are capable of aerodynamic modification of the curved side and varied cross-section sizes along the height. Twisting is another aerodynamic modification that plays a significant part in reducing the aerodynamic response. Thus, the twist angle is considered as the seventh geometric parameter. The set of aerodynamic modifications applied by these seven parameters to the basic triangular building is shown in Fig. 3.

To construct a surrogate model, a database of aerodynamic responses for several sample points is required. There are various techniques for point sampling, such as random sampling and techniques based on the principles governing the design of experiments (DOE) [34]. After specifying sample points, the aerodynamic response related to the sample points should be calculated, which the calculation can be performed via the CFD numerical method. The issue is explained in the next section.

3 CFD analysis

After creating various shapes of the buildings with trilateral cross-sections, Fluent 17.1 software was used to calculate the aerodynamic response based on the CFD numerical method. Buildings are assumed to be rigid bodies that operate as obstacles to airflow. Since there is a large number of samples whose aerodynamic response has to be calculated, and the main purpose is to obtain an approximate function to analyze the effect of exterior shape modifications of the tall buildings with trilateral cross-section on the aerodynamic response, the steady-state method is used to calculate the response.

3.1 Inflow boundary conditions

Such conditions are considered based on the equations proposed by the Architectural Institute of Japan (AIJ) recommendations. Therefore, the vertical velocity profile of U (z) and the vertical profiles of the turbulence intensity I (z) are calculated according to Eqs. 6 and 7, respectively [35].

$$U(z) = U_h\left(\frac{z}{H}\right)^{\alpha} \tag{6}$$

$$I(z) = \frac{\sigma_u(z)}{U(z)} = 0.1\left(\frac{z}{H}\right)^{(-\alpha-0.05)} \tag{7}$$

Figure 4 represents wind velocity and turbulence intensity profiles. Where U_h the velocity along the height (H) of the building and α is the exponent of the velocity profile. Assuming that the building is in the urban area, α is equal to 0.27. The velocity along the H of the building is considered 12 m/s. σ_u is the root mean square (RMS) value of velocity fluctuation across the stream-wise direction.

Concerning the convergence criterion, the level of the residuals is assumed to be 1e−5. However, this was not the mere investigation of convergence, and all forces and moments were examined in the simulations, and when they reached fixed values, convergent simulation was taken into account.

In this study, the k–ε model with Launder and Kato (LK) modification was used as the turbulence model. The model belongs to the RANS family (Reynolds Averaged Navier–Stokes equations) and provides optimal results compared to the standard k–ε model [36]. LK modification improved performance in predicting wind flow

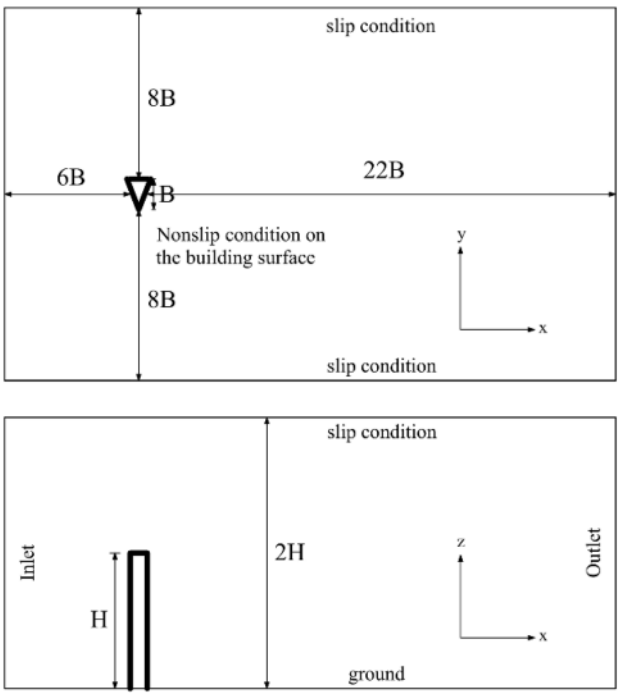

Fig. 4 Computational domain and boundary conditions

surrounding the bluff bodies [37]. The relation between I(z) and kinetic energy k(z) can be assumed as:

$$k(z) = \frac{\sigma_z^2(z) + \sigma_v^2(z) + \sigma_w^2(z)}{2} \cong \sigma_u^2(z) = (I(z)U(z))^2. \quad (8)$$

While the velocity is expressed by Eq. 6, dissipation rate via ε(z) can be calculated by Eq. 9.

$$\varepsilon(z) = C_\mu^{0.5} k(z) \frac{U_h}{z_h} \alpha \left(\frac{z}{z_h}\right)^{(\alpha-1)} \quad (9)$$

which μ is the model constant and equals to 0.09.

Other boundary conditions and computational domain are shown in Fig. 4. The computing domain 1.8 × 1.1 × 0.8 m lies along the x, y and z-axis, as shown in Fig. 4.

3.2 Mesh generation

To find the mesh configuration, several configurations are produced and the aerodynamic responses obtained from the configurations are compared, and the largest mesh size independent from the mesh grid is considered as the fine mesh. In addition, turbulent flows on the surface are investigated using the dimensionless parameter y^+ that is calculated with Eq. 10, and enable the designer to select the appropriate mesh adjacent to the walls.

$$y^+ = \frac{\rho u y}{\mu} \quad (10)$$

which ρ or air density amounts to 1.2 kg/m^3; u is friction velocity relevant to air; μ is the kinematic viscosity of air; y is vertical distance normal to wall direction.

In the current study, in all mesh grids, $y^+ < 5$. In this state, the velocity profile is considered laminar, and the viscous stress is dominant on the wall shear. Thus, enhanced wall treatment can be used, and there is no need to define wall functions [38].

4 Surrogate model

Surrogate models provide a general approximation of the output factor and can be used to better understand the relationship between the input and output factors. The aim is to replace expensive experimental tests or heavy-computational numerical simulations with a computationally smooth approximate model to simplify the analysis of complex models. The surrogate model construction is done based on regression of a limited set of observations derived from experimental and numerical simulations. For example, investigating the effect of aerodynamic modification of tall buildings on aerodynamic responses is very time consuming and costly. Figure 5 presents the flowchart for making a surrogate model for aerodynamic design. Researchers use surrogate models to circumvent such problems, explore the design space more widely, and then predict objective functions in new design points accurately and quickly without the need to the repetition of expensive simulations.

Various surrogate modeling methods have been developed to generate approximation functions for expensive numerical and experimental simulations. There are parametric and non-parametric approaches for constructing surrogate models. In parametric models (e.g., polynomial regression and Kriging), it is assumed that a global functional form is the relation between output and input factors. In contrast, in non-parametric models [such as neural network methods, and radial basis functions (RBF)], different local models are utilized in varied data regions to generate an overall model [34].

Surrogate modeling that determines the continuous function F (x) is obtained from a finite number of available data G (x) derived from experimental or numerical simulations. Where $x = [x_1, x_2, \ldots, x_n]^T$ is the vector of the input variables, and n is the number of input variables. In addition, y = F(x) represents the true responses, and $\hat{y} = G(x)$ represents the surrogate model responses, and the following equation dominates them:

$$y = \hat{y} + \varepsilon \quad (11)$$

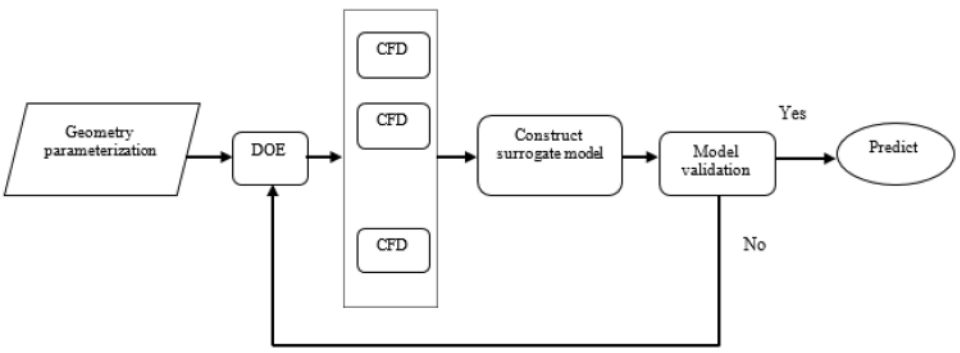

Fig. 5 Flowchart of construct surrogate model

where ε denotes the modeling and measurement errors.

To produce the surrogate model $\hat{y}$ based on different methods, a database needs to be first generated. Accordingly, some sample points in the search space has to be selected to cover the entire space. Of course, there are different sampling techniques, which some are based on the random selection in the search space, and some others are built upon the principles of Design of Experiment (DOE) such as latin hypercube sampling (LHS), central composite design, and Taguchi orthogonal array design [34, 39].

4.1 Construction of surrogate model based on polynomial regression method

Polynomial regression methodology (or response surface methodology: RSM) is a popular surrogate model with wide applications. This method approximates the all response space using a polynomial function, according to Eq. 12 [35].

$$\hat{y}(x) = \beta_0 + \sum_{i=1}^{n} \beta_i x_i + \sum_{i=1}^{n} \sum_{j>i}^{n} \beta_{ij} x_i x_j + \sum_{i=1}^{n} \beta_{ij} x_i^2 + \sum_{i=1}^{n} \sum_{j>i}^{n} \sum_{k>j}^{n} \beta_{ijk} x_i x_j x_k + \cdots + \sum_{i=1}^{n} \beta_{ii\ldots i} x_i^p \tag{12}$$

where n, number of input factors; x, vector of input factors; β, coefficients of the regression model; p, highest order of polynomials.

To construct a polynomial regression model, the unknown coefficients of β are required to be determined, and the number of β coefficients (nβ) that actually represents the number of terms considered in the regression model depends on the polynomial order and can be determined by $n_\beta = \frac{(n+p)!}{p!n!}$.

According to the least-squares law, the minimum number of sample points to determine coefficients β is nβ, and also if the number of sample points N is assumed. A matrix relation corresponding to Eq. 13 exists between X as observation data and Y as the response of corresponding data.

$$\begin{bmatrix} y^{(1)} \\ y^{(2)} \\ \vdots \\ y^{(N)} \end{bmatrix} = \begin{bmatrix} 1 & x_1^{(1)} & \cdots & x_i^{(1)} & \cdots & (x_i x_j)^{(1)} & \cdots & (x_i x_j x_k)^{(1)} & \cdots & (x_i^p)^{(1)} & \cdots \\ 1 & x_1^{(2)} & \cdots & x_i^{(2)} & \cdots & (x_i x_j)^{(2)} & \cdots & (x_i x_j x_k)^{(2)} & \cdots & (x_i^p)^{(2)} & \cdots \\ \vdots & \vdots & \ddots & \vdots & \ddots & \vdots & \ddots & \vdots & \ddots & \vdots & \\ 1 & x_1^{(N)} & \cdots & x_i^{(N)} & \cdots & (x_i x_j)^{(N)} & \cdots & (x_i x_j x_k)^{(N)} & \cdots & (x_i^p)^{(N)} & \cdots \end{bmatrix} \begin{bmatrix} \beta_0 \\ \beta_1 \\ \vdots \\ \beta_i \\ \vdots \\ \beta_{ij} \\ \vdots \\ \beta_{ijk} \\ \vdots \\ \beta_{ii\ldots i} \end{bmatrix} = \kappa\beta. \tag{13}$$

Therefore, the β coefficients are determined based on the least-squares solution of Eq. 2 using Eq. 14.

$$\beta = (\kappa^T \kappa)^{(-1)} \kappa^T Y. \tag{14}$$

After calculating the β coefficients and putting them in Eq. 1, the polynomial function is determined.

4.2 Surrogate model testing

There are various tests to evaluate the accuracy of polynomial regression models, including the root mean squared error (RMSE) test and R-Squared Coefficient (R^2), which are calculated using Eqs. 15 and 16 [39].

$$RMSE = \frac{1}{N\bar{y}} \sqrt{\sum (y - \bar{y})^2} \tag{15}$$

$$R^2 = 1 - \frac{\sum_{i=1}^{N} (y(i) - \hat{y}(i))^2}{\sum_{i=1}^{N} (y(i) - \bar{y})^2} \tag{16}$$

here $\bar{y}$ is the average value of the sample N responses. RMSE represents the accuracy of the polynomial regression model, and R^2 defines the degree of discrepancy between the polynomial model value and the true value. The closer R^2 is to one and the RMSE to zero, the model accuracy is higher.

The next parameter is R^2_{adj}, which is obtained from Eq. 17. If the value of adjusted R^2 (R^2_{adj}) is close to R^2, the terms considered in the model are correct [39].

$$R^2_{adj} = 1 - \left(\frac{D-1}{D-n}\right)(1 - R^2) \tag{17}$$

here D is the total freedom degree, and n is the number of terms taken into the model.

5 Numerical investigation

To examine the aerodynamic performance of tall buildings with trilateral cross-sections, 120 models of tall buildings with different exterior shapes were randomly generated. Then, the mean moment coefficient along the drag (C_{MD}) was calculated for each model using Eq. 18.

$$C_{MD} = \frac{M_D}{q_H B H^2} \tag{18}$$

To produce these 120 models, 30 different models were first generated using a random combination of the geometric parameters b_0, b_1, a_0, a_1, a_2, a_3, according to Fig. 6. Also Table 1 shows the numerical values of these geometric parameters.

Then, four different twist angles were considered for each of these 30 models. Afterward, the C_{MD} coefficient was calculated using the Fluent Software based on the CFD method.

Further, in building exterior shapes construction process, a set of constraints according to Eqs. 19–21 were considered to ensure the applicability of the constructed buildings in terms of architectural and structural terms.

$$0.5R \le d \le 1.5R, \quad d = b_0 + b_z \tag{19}$$

$$-30 < b_1 < 0, \quad 0^\circ \le T \le 270^\circ, \quad -30 < a_0, a_1, a_2, a_3, b_0 < 30 \tag{20}$$

$$900{,}000\ \mathrm{m}^3 \le V \le 1{,}100{,}000\ \mathrm{m}^3. \tag{21}$$

R is the radius of the circle passing through the vertices of the basic triangle and T, is twist angle. d is the maximum distance from the curve to the x-axis (see Fig. 2). The constraint $b_1 < 0$ indicates that the produced trilateral cross-sections have merely convex curvature. V is the volume of the building with a 10% tolerance for its variations.

Since the direction of the wind load on the building is not specified, four different angles of attacks (AOAs) were considered in accordance with Fig. 7. Furthermore, given the cross-section is symmetrical, it was assured that four intended AOAs cover a total of 12 states of wind load angles with a 30° interval. Finally, the C_{MD} response for the four AOAs was calculated, and the maximum response was considered as the final response of the model.

5.1 Validation

To perform validation, the base triangular building is analyzed using the turbulence model k–ε modified by LK method, and a comparison is made between the velocity and turbulence intensity profile in the position of the building model with the experimental results presented by Mukherjee et al. [40] (see Fig. 8). Mukherjee et al. investigated the effect of the external shape of tall buildings on aerodynamic responses using experimental and numerical results. They also used the RANS model in their study to simulate turbulence. In the paper, the considered

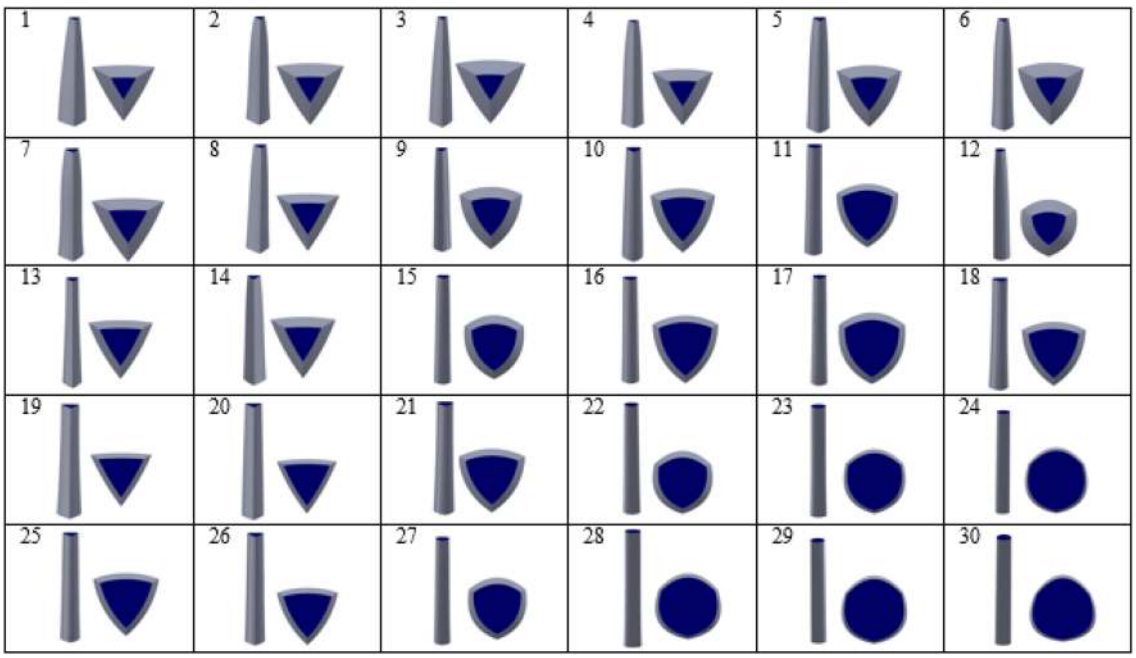

Fig. 6 Thirty different tall building geometries for an aerodynamic database generation

Table 1 The numerical values of the geometric parameters

Model	a_0	a_1	a_2	a_3	b_0	b_1
1	0.37	− 1.46	5.77	− 8.10	0.21	− 0.96
2	0.17	− 0.41	1.28	− 2.60	0.10	− 1.32
3	29.75	− 15.44	8.64	− 11.57	21.14	− 1.91
4	0.02	− 0.04	− 19.20	− 0.26	0.01	− 1.84
5	0.90	− 0.95	− 3.81	1.69	0.52	− 1.32
6	− 0.35	0.83	− 1.22	0.33	− 0.21	− 1.32
7	1.84	− 7.84	29.63	− 28.56	1.06	− 1.84
8	1.85	− 6.52	28.43	− 26.54	1.06	− 1.84
9	0.90	− 0.95	− 3.81	1.69	0.54	− 2.35
10	1.85	− 4.21	1.83	4.57	1.06	− 1.84
11	0.87	− 2.38	10.12	− 23.05	0.54	− 2.35
12	0.02	− 0.07	0.31	− 0.63	0.01	− 4.49
13	− 2.31	5.41	− 20.53	27.41	− 1.48	− 4.51
14	1.51	− 3.22	8.79	− 12.13	1.14	− 4.57
15	1.51	− 3.22	8.79	− 12.13	1.15	− 5.17
16	0.18	− 0.19	− 0.23	0.13	0.12	− 5.64
17	1.77	− 4.15	6.12	− 1.65	1.21	− 6.89
18	0.18	− 0.41	0.61	− 0.16	0.12	− 7.08
19	28.35	− 29.55	0.13	− 0.26	0.01	− 6.89
20	0.30	− 0.64	1.76	− 2.43	0.25	− 8.01
21	− 0.15	0.32	− 0.88	1.21	− 0.13	− 9.48
22	− 0.15	0.32	− 0.88	1.21	− 0.14	− 11.76
23	1.13	− 2.63	7.90	− 13.27	0.94	− 11.56
24	0.23	− 0.48	1.32	− 1.82	0.21	− 14.13
25	1.57	− 2.71	10.36	− 29.38	0.14	− 13.18
26	− 1.51	3.22	− 8.79	12.13	− 1.49	− 16.27
27	0.13	− 0.35	1.28	− 1.56	0.16	− 18.55
28	2.28	− 6.03	21.70	− 26.57	2.81	− 21.73
29	1.14	− 0.61	0.33	− 1.49	0.17	− 23.67
30	1.14	− 0.61	0.33	− 1.49	0.19	− 28.44

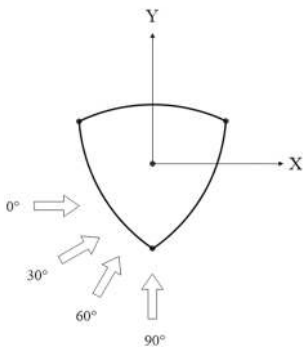

Fig. 7 The wind direction on the building

boundary conditions are similar to those of the present article.

5.2 Grid convergence study (GCS)

The GCS process is based on the principle that as the fineness of the grids increases, spatial separation errors asymptotically approach zero, thus helping to achieve grid-independent responses. Richardson extrapolation (RE) method was used for discretization error estimation [41], which is currently one of the most reliable methods available for predicting numerical uncertainty [42].

In the present study, grid convergence index (GCI) method that is based on RE as an acceptable and recommended method was used to produce a mesh grid with both good accuracy and low computational cost [42]. In this process, as shown in Fig. 9 four different levels of grid with structured mesh (i.e. coarse, medium, fine, and very fine) were produced, and the number of cells systematically increased. And the moment coefficient responses corresponding to these grids are equal to, 0.351, 0.290, 0.285 and 0.281 respectively. Therefore,

the results show that the aerodynamic response of the moment coefficient converges with the structured mesh G3 with 0.71 error percentage. As a result, the grid is selected as the optimal grid, and the details of the grid configuration are shown in Fig. 10.

5.3 Regression model

Ultimately, these 120 different models were used as the sample points in order to fit an appropriate regression model. Now, for statistical analysis, seven geometrical parameters were considered as the input factors, and the aerodynamic response (C_{MD}) was regarded as the output factor. Then, the effects of main factors, power factors and factors interaction were investigated using the forward

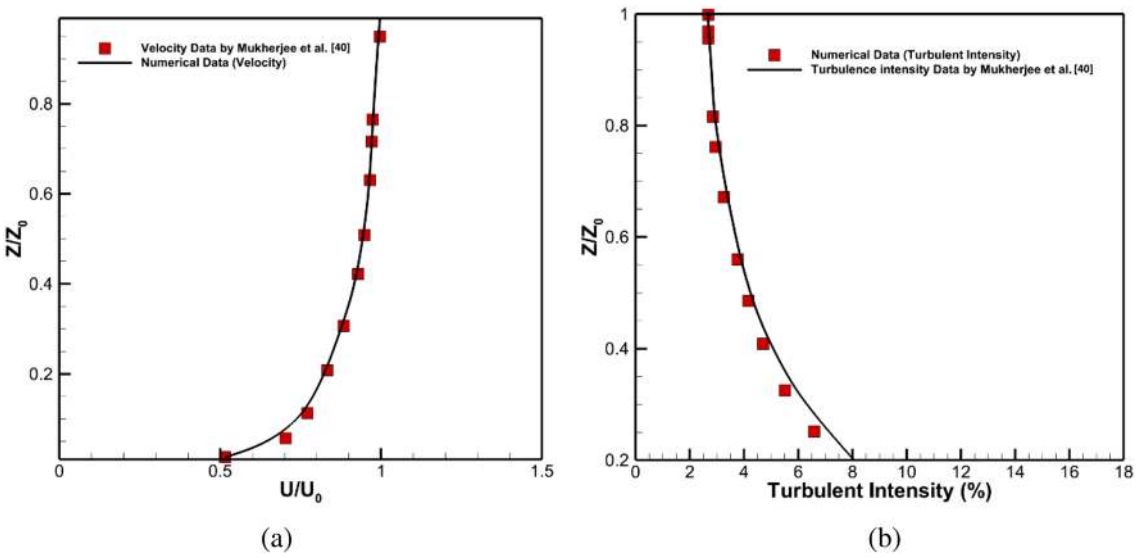

Fig. 8 Comparison of wind velocity and turbulence intensity predicted by experimental and numerical results: **a** wind velocity, **b** turbulence intensity

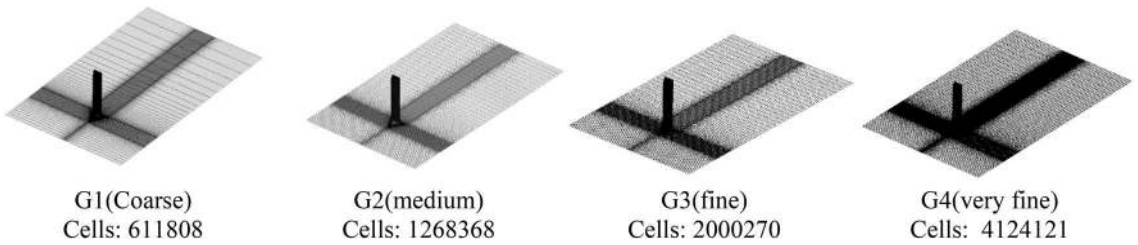

Fig. 9 Four different grid configuration

Fig. 10 Grid generation detail

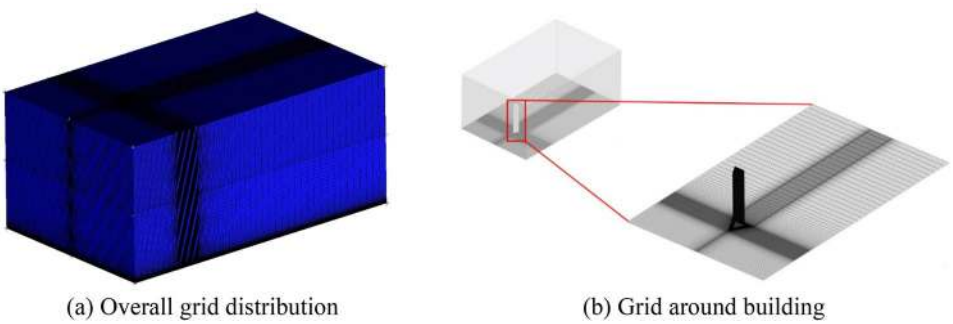

method selection regression method as an efficient method for non-regular design [39]. Then, by screening the main factors, we obtain *P* values for all main factors (see Table 2). As can be seen, the two main factors, b1 and T, have the lowest *P* value, thus they can significantly affect the aerodynamic response. This indicates that the two aerodynamic modifications, namely "curved sides" and "twisting", which are applied to the exterior shape of the building using two factors b_1 and T have the greatest effect on the C_{MD} coefficient. Finally, the explicit equation was obtained between these two geometrical parameters and the moment coefficient (C_{MD}) based on Eq. 22. This relation helpfully enables designers to evaluate the effect of geometrical parameters on the response of tall buildings with trilateral cross-sections with low computational cost and more facile.

The proposed model has the R-squared (R^2) value of 0.912 and adjusted R^2 (R^2_{adj}) 0.906. The proximity of the value of these two coefficients indicates the correctness of the intended terms (8 terms in Eq. 9) in the model. In addition, the RMSE value is 0.0574, which is not significant. Table 3 shows the results of the analysis of variance (ANOVA). The *P* value indicates that the model and all considered terms are significant at level 1% ($\alpha = 0.01$), except for the T term, which is significant at level 5%. Furthermore, the lack of fit (LOF) is not significant, all of which indicate that the model has a high ability to approximate the aerodynamic response.

The second column "Estimate", shows the model coefficients, which are the same coefficients C_1–C_8 used in Eq. 22.

$$\begin{aligned} C_{MD} &= C_1 b_1^3 + C_2 b_1^2 + C_3 b_1 + C_4 T^3 + C_5 T^2 + C_6 T + C_7 b_1 T + C_8 \\ C_1 &= -6.29\text{E}-05, C_2 = -0.0026, C_3 = 0.0056, C_4 = -1.58\text{E}-08, C_5 = 1.14\text{E}-05 \\ C_6 &= -0.00318, C_7 = -5.45\text{E}-05, C_8 = 1.29149603 \end{aligned} \tag{22}$$

5.4 Analytical optimization

Equation 22 represents a surface in 3D space, and Fig. 11 shows the surface produced by this equation. This 3D plot helps designers to schematically investigate the effect of input factors b_1, T on C_{MD} output factor. As can be seen from Fig. 8, the coefficient b_1 strongly affects the C_{MD}, such that decreasing b_1 decreases the coefficient of C_{MD} with a very steep slope, which indicates that with an increase in the curvature of the cross-section sides, the C_{MD} coefficient as the intended aerodynamic response is greatly reduced. The next influencing factor is the T factor. As can be seen in the Fig. 11, by increasing the twist angle to about 90°, the C_{MD} coefficient value decreases

Table 2 Screening of main factors

Parameter	*P* value
Intercept	1.000
a_0	0.940
a_1	0.635
a_2	0.882
a_3	0.645
b_0	0.981
b_1	2.20E−41
T	2.80E−10

Table 3 Analysis of variance (ANOVA)

Source of variation	Estimate	Sum of squares	Degrees of freedom	F_0	*P* value
Intercept	1.29149603	–	–		–
Model	–	5.76268	7	0.82324	< 0.0001
b1	0.005605218	1.75661	1	1.75661	< 0.0001
b1 * T	−5.45E−05	0.31163	1	0.31163	< 0.0001
T * T	1.14E−05	0.18577	1	0.18577	< 0.0001
b1 * b1 * b1	− 6.29E−05	0.08815	1	0.08815	< 0.0001
b1 * b1	− 0.00264683	0.08046	1	0.08046	< 0.0001
T * T * T	− 1.58E−08	0.03312	1	0.03312	0.0017
T	− 0.003184352	0.02047	1	0.02047	0.0126
Lack of fit	–	0.30964	103	0.00301	0.9113
Pure error	–	0.04714	9	0.005237	–
Total	–	6.11947	119	0.051424	–

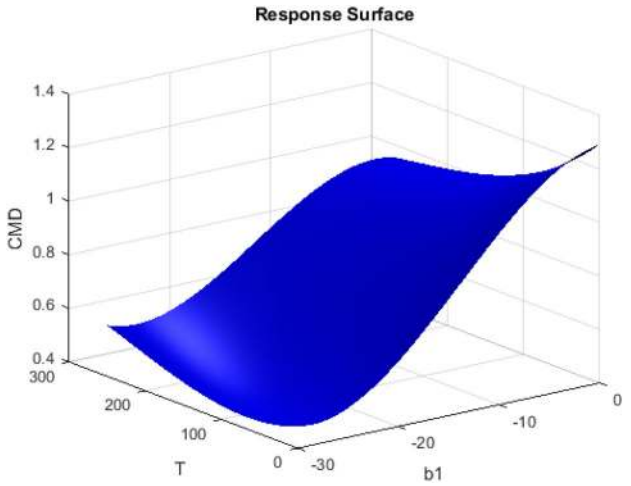

Fig. 11 Response surface of building moment coefficient to two factors

and then increases. Finally, using the first derivative test method, the T and b_1 values corresponding to the minimum value of the C_{MD} coefficient are calculated.

Here, the derivatives of the C_{MD} equation with respect to variables b_1 and T are separately obtained according to Eqs. 23 and 24. Then, by putting each of the equations equal to zero, the extreme points of the C_{MD} equation is calculated.

$$\frac{\partial C_{MD}}{\partial T} = -0.00474T^2 + 2.28T - 5.45b_1 - 320 = 0 \quad (23)$$

$$\frac{\partial C_{MD}}{\partial b_1} = -18.870b_1^2 - 530b_1 - 5.45T + 560 = 0 \quad (24)$$

Now, by solving this system that is comprised of two equations and two unknowns, the following values are obtained for factors T and b_1.

$$b_1 = \left\{ \begin{array}{c} -28.199 \\ -24.841 \end{array} \right\}, T = \left\{ \begin{array}{c} 90 \\ 270 \end{array} \right\} \quad (25)$$

The above equations system has four solutions for each factor, two of which are real (shown above), and the remaining two are complex solutions that not considered. The four real pairs (b_1, T), which are the critical points of the C_{MD} function, are put into Eq. 22, separately, and their corresponding C_{MD} responses are calculated and compared.

$$F(b_1, T) = F(-28.199, 90) = 0.3717, F(-28.199, 270) = 0.5125$$
$$F(-24.841, 90) = 0.3992 F(-24.841, 270) = 0.5080$$

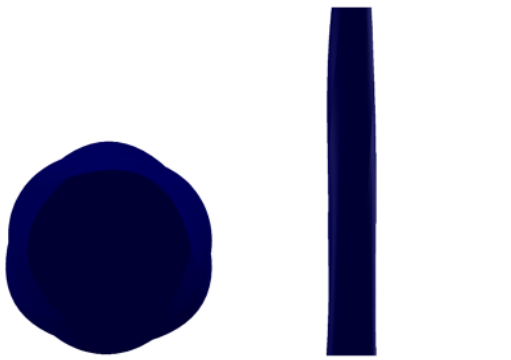

Fig. 12 A sample of optimal shape with geometric parameters {a_0, a_1, a_2, a_3, b_0, b_1} = {0.013, − 0.030, 0.277, − 0.660, 0.016, − 28.199, 90}

According to the calculated C_{MD} values for the four above points, the point (b_1, T) = (− 28.199, 90) has the lowest C_{MD} coefficient of 0.3717, which represents the minimum point of the C_{MD} function. The building with these geometrical parameters benefits from the best aerodynamic performance. A sample of the optimal shapes of the tall buildings is presented in Fig. 12. C_{MD} value calculated by the CFD method for the sample is 0.3542 (for AOA = 60^0), which indicates the accuracy of the proposed approximate function in calculating the C_{MD}.

The C_{MD} coefficient value for the basic triangular building was obtained using CFD analysis to be 0.842. In fact, the aerodynamic response value of the optimal building has decreased by about 56% compared to the basic triangular building. Therefore, the aerodynamic modifications inflicted to exterior shape of the building can greatly reduce construction costs.

Figure 13 shows the mean velocity contour of the wind flow for sample 1 and basic shape obtained from CFD simulations. Shape modifications change the flow pattern around the tall buildings and the wake zone in the optimal shape is significantly smaller than the basic triangular shape. Which indicates an improvement in the aerodynamic performance of the optimal shape compared to the base triangular building.

The effect of both factors b_1 and T on the C_{MD} coefficient is investigated in the graph of Fig. 14. As can be seen, the effect of these two factors is evaluated on the C_{MD} coefficient when they are at their upper and lower levels. Accordingly, when the twist angle is at its low level, the coefficient b_1 strongly influences the C_{MD} response, and by decreasing b_1 the coefficient C_{MD} decreases with a steep slope. On the other hand, when the coefficient b_1, is at its high level, the C_{MD} response decreases with increasing twist angle.

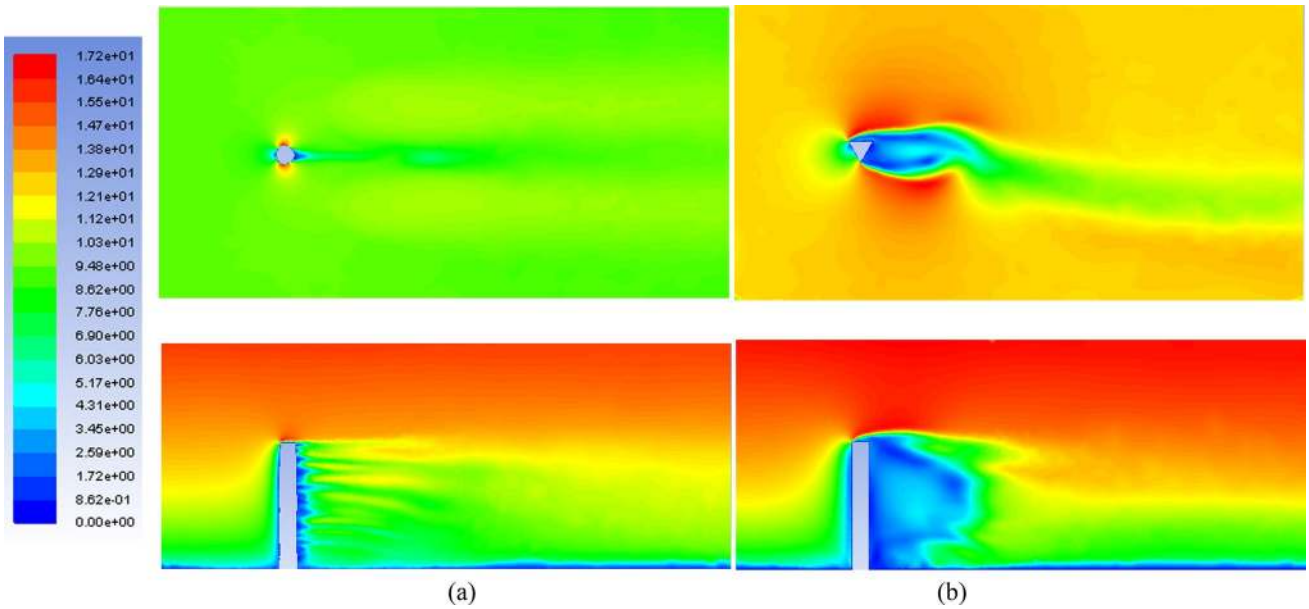

Fig. 13 Flow field around building at z = H/2: **a** optimal shape and **b** basic triangle shape

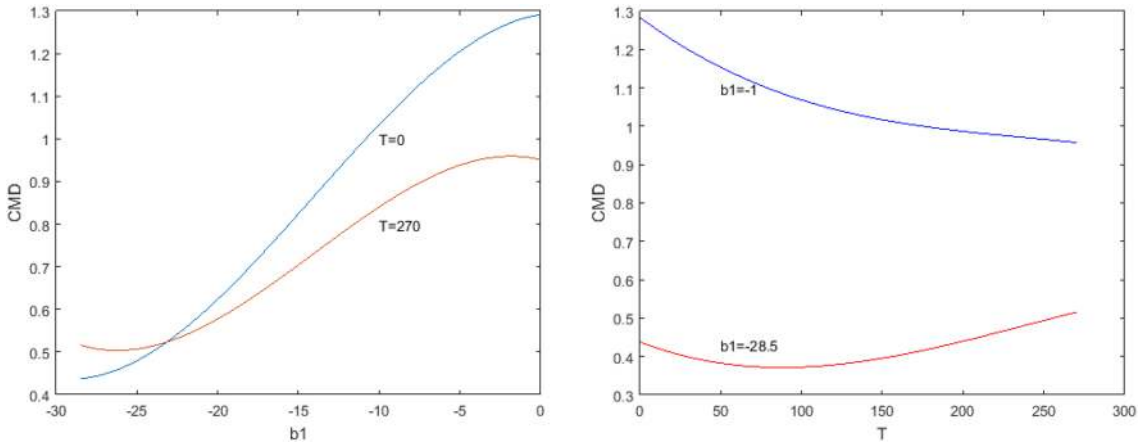

Fig. 14 The effect of factors on the moment coefficient

6 Conclusion

The current research provided an explicit function for the moment coefficient of the tall buildings with trilateral cross-sections as a surrogate model instead of CFD analysis. Benefitting from $R^2 = 0.912$ coefficient, the function is based on the polynomial regression method in terms of two geometrical parameters b_1 and T, and it is capable of approximating the C_{MD} coefficient of tall buildings with an acceptable level of accuracy. The paper enables building designers to study impact of aerodynamic modifications of tall building exterior shape on the CMD response easily and with minimal computational cost. In addition, the results provide the designers with the opportunity to explore the desired exterior shape in the wide search space. Finally, by obtaining the extreme points of this function, it was found that by considering the values of − 28.199 and 90 for b_1 and T, respectively, the lowest response $C_{MD} = 0.3717$ and optimal aerodynamic performance of tall buildings with trilateral cross-sections can be obtained. In addition, The C_{MD} coefficient decreased by about 56% compared to the basic triangular building, indicating the importance of the exterior shape effect in reducing building aerodynamic response and consequently lowering its construction costs.

Compliance with ethical standards

Conflict of interest On behalf of all authors, the corresponding author states that there is no conflict of interest.

References

1. Xiang H, Ge Y (2007) Aerodynamic challenges in span length of suspension bridges. Front Archit Civ Eng China 1(2):153–162
2. Katsuchi H et al (2016) Improvement of aerodynamic stability of suspension bridges with H-shaped simplified stiffening girder. Front Struct Civ Eng 10(1):93–102
3. Tamura T, Miyagi T (1999) The effect of turbulence on aerodynamic forces on a square cylinder with various corner shapes. J Wind Eng Ind Aerodyn 83(1–3):135–145
4. Tamura T, Miyagi T (1998) Kitagishi, Numerical prediction of unsteady pressures on a square cylinder with various corner shapes. J Wind Eng Ind Aerodyn 74:531–542
5. Gu M, Quan Y (2004) Across-wind loads of typical tall buildings. J Wind Eng Ind Aerodyn 92(13):1147–1165
6. Tse K-T et al (2009) Economic perspectives of aerodynamic treatments of square tall buildings. J Wind Eng Ind Aerodyn 97(9–10):455–467
7. Hayashida H, Iwasa Y (1990) Aerodynamic shape effects of tall building for vortex induced vibration. J Wind Eng Ind Aerodyn 33(1–2):237–242
8. de Macedo Wahrhafig A, da Silva MA (2018) Using computational fluid dynamics to improve the drag coefficient estimates for tall buildings under wind loading. Struct Des Tall Spec Build 27(3):e1442
9. Kim Y, Kanda J (2010) Characteristics of aerodynamic forces and pressures on square plan buildings with height variations. J Wind Eng Ind Aerodyn 98(8–9):449–465
10. Kim Y-M, You K-P, Ko N-H (2008) Across-wind responses of an aeroelastic tapered tall building. J Wind Eng Ind Aerodyn 96(8–9):1307–1319
11. Xie J (2014) Aerodynamic optimization of super-tall buildings and its effectiveness assessment. J Wind Eng Ind Aerodyn 130:88–98
12. Cooper K et al (1997) Unsteady aerodynamic force measurements on a super-tall building with a tapered cross section. J Wind Eng Ind Aerodyn 72:199–212
13. Kim Y-M, You K-P (2002) Dynamic responses of a tapered tall building to wind loads. J Wind Eng Ind Aerodyn 90(12–15):1771–1782
14. Kim YC, Kanda J (2013) Wind pressures on tapered and set-back tall buildings. J Fluids Struct 39:306–321
15. Kim YC, Kanda J, Tamura Y (2011) Wind-induced coupled motion of tall buildings with varying square plan with height. J Wind Eng Ind Aerodyn 99(5):638–650
16. Bairagi AK, Dalui SK (2020) Forecasting of wind induced pressure on setback building using artificial neural network. Period Polytech Civ Eng 64(3):751–763
17. Kumar B et al (2012) Local and total wind force characteristics of triangular-section tall buildings. In: Proceedings of the 22nd national symposium on wind engineering
18. Dutton R, Isyumov N (1990) Reduction of tall building motion by aerodynamic treatments. J Wind Eng Ind Aerodyn 36:739–747
19. Miyashita K et al (1993) Wind-induced response of high-rise buildings effects of corner cuts or openings in square buildings. J Wind Eng Ind Aerodyn 50:319–328
20. Okada H, Kong L (1999) The effects of open passage on reducing wind response of tall building. In: Proceedings of the 29th Technical Report. Tokyo. Public Works Research Institute, pp 561–566
21. Tanaka H et al (2012) Experimental investigation of aerodynamic forces and wind pressures acting on tall buildings with various unconventional configurations. J Wind Eng Ind Aerodyn 107:179–191
22. Tamura Y et al (2013) Aerodynamic and response characteristics of super-tall buildings with various configurations. In: Proceedings of the 8th Asia-Pacific conference on wind engineering, Chennai, India
23. Bandi EK et al (2013) Experimental investigation on aerodynamic characteristics of various triangular-section high-rise buildings. J Wind Eng Ind Aerodyn 122:60–68
24. Daemei AB et al (2019) Study on wind aerodynamic and flow characteristics of triangular shape tall buildings and CFD simulation in order to assess drag coefficient. Ain Shams Eng J 10:541–548
25. Kareem A, Spence SMJ. Bernardini E, Bobby S, Wei D (2013) Using computational fluid dynamics to optimize tall building design. In: CTBUHJ (III), pp 38–42
26. Elshaer A, Bitsuamlak G (2018) Multiobjective aerodynamic optimization of tall building openings for wind-induced load reduction. J Struct Eng 144(10):04018198
27. Elshaer A, Bitsuamlak G, El Damatty A (2017) Enhancing wind performance of tall buildings using corner aerodynamic optimization. Eng Struct 136:133–148
28. Bernardini E et al (2015) Aerodynamic shape optimization of civil structures: A CFD-enabled Kriging-based approach. J Wind Eng Ind Aerodyn 144:154–164
29. Krajnovic S (2007) Aerodynamic optimization of vehicles using computational fluid dynamics and response surface methodology. In: Proceedings of the XXI international automotive conference science & motor vehicles, Beograd, 23–24 April 2007
30. Lu H, Zheng X, Li Q (2014) A combinatorial optimization design method applied to S-shaped compressor transition duct design. Proc Inst Mech Eng Part G J Aerosp Eng 228(10):1749–1758
31. Immonen E (2017) 2D shape optimization under proximity constraints by CFD and response surface methodology. Appl Math Model 41:508–529
32. Nariman NA (2017) Kinetic energy based model assessment and sensitivity analysis of vortex induced vibration of segmental bridge decks. Front Struct Civ Eng 11(4):480–501
33. Samareh A, Jamshid A (1999) A survey of shape parameterization techniques. NASA Langley International Forum on Aeroelasticity and Structural Dynamics
34. Yondo R, Andrés E, Valero E (2018) A review on design of experiments and surrogate models in aircraft real-time and many-query aerodynamic analyses. Prog Aerosp Sci 96:23–61
35. Tominaga Y et al (2008) AIJ guidelines for practical applications of CFD to pedestrian wind environment around buildings. J Wind Eng Ind Aerodyn 96(10–11):1749–1761

36. Kato M (1993) The modelling of turbulent flow around stationary and vibrating square cylinders. Turbulent Shear Flow 1:10.4.1–10.4.6
37. Huang S, Li Q, Xu S (2007) Numerical evaluation of wind effects on a tall steel building by CFD. J Constr Steel Res 63(5):612–627
38. Fluent (2005) Documentation: User Guid, Ansys Inc
39. Montgomery DC (2017) Design and analysis of experiments. Wiley, New York
40. Mukherjee S et al (2014) Wind induced pressure on Y plan shape tall building. Wind Struct J 19(5):523–540
41. Celik IB et al (2008) Procedure for estimation and reporting of uncertainty due to discretization in CFD applications. J Fluids Eng Trans ASME 130(7):371–380
42. Sanyal P, Dalui SK (2020) Comparison of aerodynamic coefficients of various types of Y-plan-shaped tall buildings. Asian J Civ Eng 21(1):1109–1127